INTERACTION BETWEEN TURBULENT DYNAMICAL PROCESSES AND STATISTICS IN DEFORMED AIR-LIQUID INTERFACES, VIA DNS

Yoshinobu Yamamoto
Department of Nuclear Engineering,
Kyoto University
Yoshida Sakyo Kyoto, 606-8501, Japan
yyama@nucleng.kyoto-u.ac.jp

Tomoaki Kunugi
Department of Nuclear Engineering,
Kyoto University
Yoshida Sakyo, Kyoto 606-8501, Japan
kunugi@nucleng.kyoto-u.ac.jp

ABSTRACT

The present study investigates the effects of a surface deformation on near free-surface turbulent structures, by means of direct numerical simulation (DNS). Target flow fields are two different types of air-liquid interface turbulent shear flows. One flow filed is a wind-driven turbulent flow at maximum wind speed of 2.2m/s. The other one is an air-liquid counter current flow induced by a high-speed liquid film at Froude number of 1.8 based on the bulk mean velocity and the wave velocity of a long wave. In the wind-driven flow, turbulent intensity distributions and theirs redistributions in the vicinity air-liquid interfaces are strongly influenced by the wind-wave shapes. On the other hands, vertical turbulent intensity in the open-channel flow has the peak value on the free-surface and a vertical confinement effect in a low-Fr flow is no longer present in this high-Fr flow. Beneath the air-liquid interface, turbulence redistribution form vertical component to streamwise one is dominant in both cases.

INTRODUCTION

In the view point of free-surface turbulence modelling, turbulent flows with air-liquid interfaces could be classified into two flow-types based on the absence or presence of air-liquid interface interactions.

An open-channel turbulent flow is one of the air-liquid interface interaction inactive-flows. In an open-channel flow, Froude number [Fr = $U_b/(gh)^{1/2}$, where U_b is bulk velocity, g is gravity acceleration and h is flow depth] was an impact factor for free-surface deformation effects on turbulent structures.

On the other hands, a response between atmosphere and ocean is one of most famous turbulent flows induced by air-liquid interactions. In an atmosphere-ocean interaction, momentum transfer would be conducted by way of drag effects of a wind on an ocean surface. A wave and water current caused by this drag effects of a wind, is called a wind-wave and wind-driven current, respectively.

Main objective of this study is to estimate the surface deformation effects on turbulence structures for two different types of air-liquid interface turbulent shear flows by using the MARS (Multi-Interfaces Advection and Reconstruction Solver) method (Kunugi,2001), which was the direct numerical solution procedure of a coupled gas-liquid turbulent flow. One target flow filed is a fully-developed wind-driven turbulent flow at the maximum wind speed 2.2m/s. The other is an air-liquid counter current flow induced by a high-speed liquid film for Fr=1.8; “Super-critical turbulent open-channel flow”. As the results, we can obtain the turbulent statistics beneath the deformed free-surface and we compare the turbulent structures in the view points of the free-surface turbulence modelling.

NUMERICAL PROCEDURES

Numerical procedure was based on the MARS method (Kunugi, 2001); governing equations are Navier-Stokes equations with the CSF (Continuum Surface Force) model (Brackbill et al., 1992), continuity equation, transport equations of a volume fraction function F, respectively.

Regarding the discretization of the velocity fields on the Cartesian coordinate system, the second-order scheme for the spatial differencing terms is used on the staggered grid system. The time integration method is based on the fractional-step method25 and the third-order low-storage Runge–Kutta scheme is adapted for the convection terms, the Crank–Nicolson scheme is adapted for the viscous term and the Euler implicit scheme for the pressure term. Fractional-step velocity is obtained by solving the momentum equations using the conjugate residual (CR) method, and the following Poisson equation is solved by the incomplete LU biconjugate gradient (ILUBCG) method.

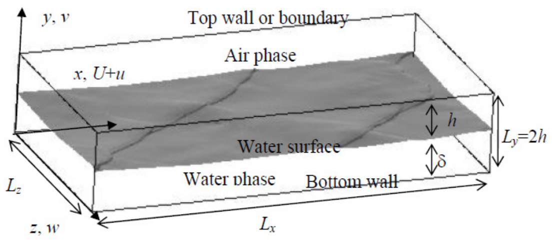

U: streamwise mean velocity, u,v,w: turbulent velocity for stream (x)-, vertical (y)-, and span (z)- wise directions.

Figure 1. Computational domain and coordinate system

NUMERICAL CONDITION

The physical problem treated here is the motion of two Newtonian incompressible fluids allowed the interface deformation between them. In Fig.1, the schematic view is shown, where U is the streamwise mean velocity, u,v,w are the turbulent velocity in streamwise-, vertical- and spanwise-directions, and h is gas layer height (= δ:flow depth). Numerical conditions of the present two DNSs are shown in Table 1, where CASE1 is of a fully-developed wind-driven turbulent flow, CASE2 is of a super-critical open-channel flow.

In CASE1 (wind-driven flow), the periodic boundary conditions in the spanwise (x) and streamwise (z) directions are imposed, free-slip condition is applied to the upper boundary of gas-phase and the no-slip condition is imposed on the lower boundary of water-phase. As the initial conditions, the water surface is flat, velocity fields for gas layer are used the DNS result of fully-developed turbulent boundary layer flow at the turbulent Reynolds number 150 (Yamamoto et al., 2001) and for water layer also used one hundredth of that flow field. Constant streamwise mass flux condition for gas side and zero pressure gradient in water side i.e., water flow is driven by the gas flow are applied. All data were normalized by the initial air-side friction velocity and kinetic viscosity. Superscript + denotes the dimensionless quantities normalized by them.

In CASE2 (super-critical open-channel flow, Yamamoto et. al, 2006), the periodic boundary conditions in the spanwise (x) and streamwise (z) directions are imposed, the no-slip condition is applied to upper boundary of gas-phase and lower boundary of water-phase. As the initial conditions, the water surface was flat. All data were normalized by the initial bottom-wall friction velocity and water-phase kinetic viscosity. Superscript + also denotes the dimensionless quantities normalized by them.

RESULTS AND DISSCUSSION

Water-surface characteristics

Figures 2 show mean velocity profiles and instantaneous water-surface distributions in the wind-driven flow and the super-critical open-channel flow. The mean velocity profile of the wind-driven flow shows that the gas-side flow drags the water-side flow like a Couette flow as shown in Fig.2-(a). In the wind-driven flow, some wind-waves with the crests and these wind-waves are formed the large scale-shapes in the horizontal directions.

In Fig.2-(b), the mean velocity profile of the super-critical open-channel flow shows that the air- and water-side flow into the countercurrent direction each other but the air-side flow near free-surface is following to the water-side flow. The mean velocity profile of the air-side flow shows the parabolic one. This means that the air-side flow is not a turbulent flow but a laminar flow. In the super-critical open-channel flow, gently bumped waves and high-frequency fluctuations on them are observed.

Figures 3 show the water-surface turbulent intensity profiles. The turbulent intensity profile of the wind-driven flow are asymmetrical at initial water-surface position y^+ = 150 in

Table 1 Numerical condition

CASE	Re_τ	ρ_w/ρ_g	Domain $L_x \times L_y \times L_z$	Grid number $N_x \times N_y \times N_z$	Resolution $\Delta x^+, \Delta y^+, \Delta z^+$	T_0^+	T_1^+
CASE1	150	842.1	$10h \times 2h \times 5h$	256×164×256	5.86, 0.26-4.56,2.93	4210	800
CASE2	150	842.1	$12.8h \times 2h \times 6.4h$	384×214×192	5.00, 0.26-2.00,5.00	610	730

CASE1 (wind-driven flow):
$Re_\tau = u_\tau h/\nu_g$: Turbulent Reynolds number, u_τ: Friction velocity at air-liquid interface in initial condition, h: Gas Layer height, ν_g: Kinetic viscosity of air,
ρ_w : liquid density, ρ_g : Air density, σ: coefficient of surface tension
L_x, L_y, L_z: Computational domain,Nx, Ny, Nz: Grid number,
Δx^+,Δy^+,Δz^+: Grid resolution for stream (x)-, vertical (y)-, and span (z)- wise directions.
Super-script + denotes the nondimensional quantities normalized by friction velocity and kinetic viscosity used Reynolds number definition.
T_0^+: Time integration length from initial condition to fully-developed status,
T_1^+: Time integration length after fully-developed status.
CASE2 (super-critical open-channel flow):
$Re_\tau = u_\tau \delta/\nu_w$: Turbulent Reynolds number, u_τ: Friction velocity at bottom wall, δ=h: water depth, ν_w: Kinetic viscosity of water

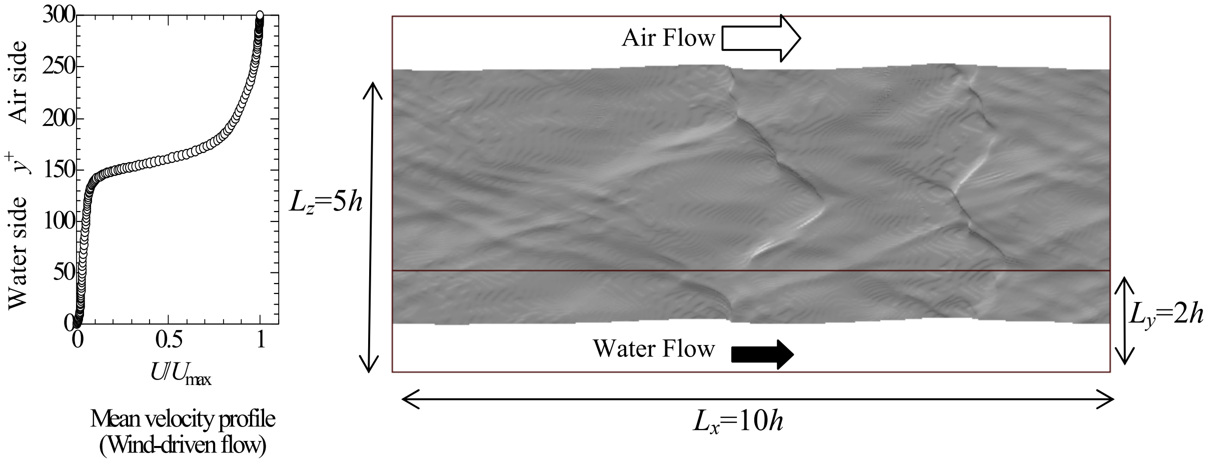

(a) wind-drivent flow

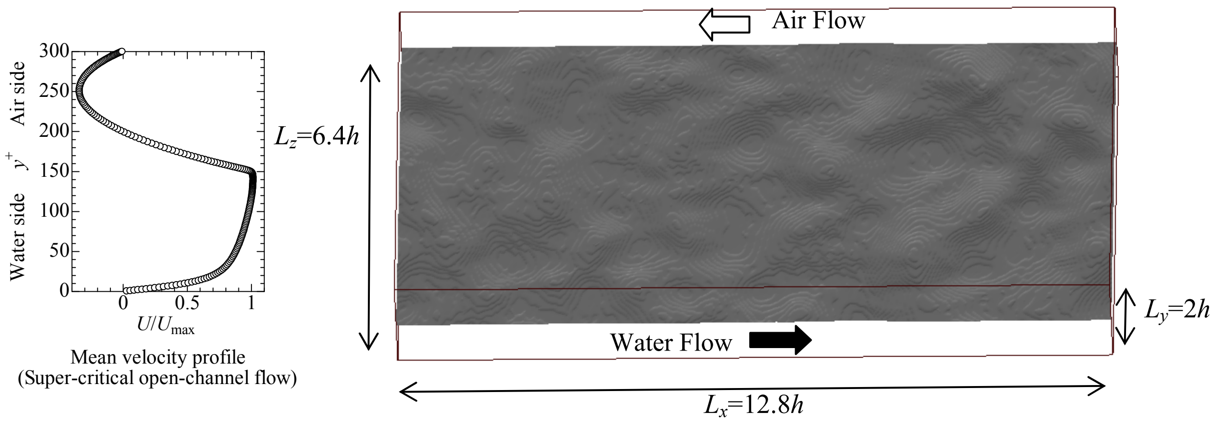

(b) open-channel flow

Figure 2. Mean velocity profiles and instantaneous air-liquid interface characteristics.

Fig.3-(a). This is why that the wind-wave profiles, which have the crest leaned toward the leeward. On the other hand, that of the super-critical open-channel flow is almost symmetrical as shown in Fig.3-(b).

Figures 4 are the streamwise spectrum of VOF function F. The spectrum of the wind-driven flow is followed –4th power law in the low wave-number range. This tendency of spectrum profile in low-wave number range is good agreement with the observational result at ocean (Kawai, 1979).

That of the super-critical open-channel flow has the one peak derived from the gently bumped waves as shown in Fig.2-(b).

Turbulent intensity in wind-driven flow

Figures 5 show the turbulent intensity profiles in the wind-driven flow. Note that these data were averaged at the height from the bottom wall and distinguished the air-phase from the water-phase, i.e. the air- and water-phase mean and statistics values are calculated in the surface-deformation area.

In the wind-driven flow, water-phase turbulent intensities are decreased close to the air-liquid interfaces, and all water-phase turbulent intensities have the peak values, however these positions are different from others.

The vertical turbulent intensity has the peak value at lowest height corresponded to the initial interface position ($y^+ = 150$). This indicates that the fluctuations of vertical velocity component are caused by the wind-waves. Therefore, vertical confinement effects as well as the low Froude number open-channel flows would be present in the wind-driven flow.

The peak height of the spanwise turbulent intensity is highest than those of others. Not only the vertical but also the streamwise confinement effects seem to exist, because the wind-waves have the crest leaned toward the leeward.

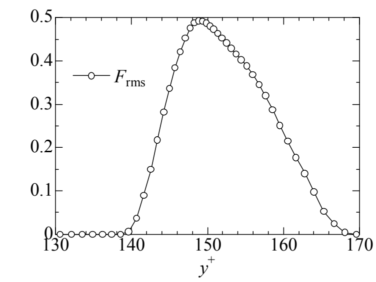

R.M.S. of VOF function distributions
(Wind-driven flow)

(a) wind-drivent flow

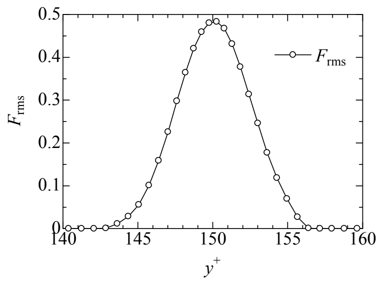

Profile of averaged R.M.S. of *F*,
near free-surface (Fr=1.8)

(b) open-channel flow

Figure 3. R.M.S. of volume of fluid (VOF) function profiles.

Figure 6 shows the velocity distributions and air-liquid interface profiles in the wind-driven flow.

In Figs. 6-(a) and (d), high and low speed streaky structures as well as non-deformed air-liquid interface turbulent flow result (Angelis and Banerjee, 1996), are observed in both gas-and water-side, however these streaks seem to be blocked by the wind-waves as shown in Figs.6-(a),(b), and (d). The vertical turbulence in Fig.6-(c) shows a strong correlation with the wind-waves.

Turbulent intensity in open-channel flow

In the super-critical open-channel flow (Fig.7), near the free-surface (y^+ > 140), vertical turbulent intensity begins to increasing up to the free-surface and free-surface vertical confinement effect (Komori et al., 1982) is no longer observed. This indicates that near free-surface turbulence is caused by the free-surface instabilities. In this supercritical open-channel flow, Yamamoto and Kunugi, 2010 was confirmed that the energy dissipation rate was also increased toward the free-surface and the redistribution of the turbulent kinetic energy was in good agreements with the previous experimental correlation proposed by Nezu 2005.

Redistribution of turbulent intensities

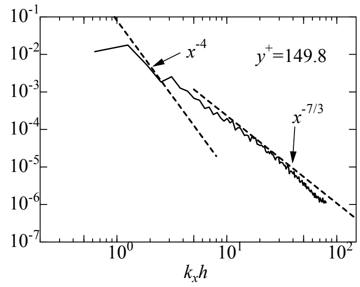

Streamwise energy spectra of VOF function

(a) wind-drivent flow

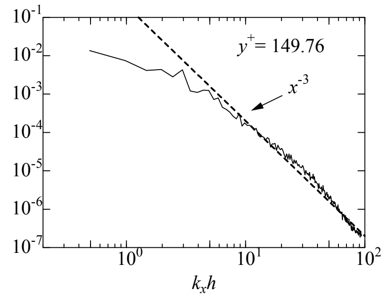

Streamwise energy spectra of VOF function

(b) open-channel flow

Figure 4. 1D energy spectrum of VOF function at the air-liqud interface.

Figure 8 shows pressure-strain term distributions, where φ_{11}, φ_{22}, φ_{33} denotes the streamwise, vertical and spanwise pressure-strain term, respectively. In the wind-driven flow (Fig.8-(a)), the redistribution from the vertical pressure-strain term to streamwise one is observed in all the surface deformation area. Near the crest of the wind-waves (y^+>160), the spanwise pressure-strain term contribution shows a sharp increase and exceeds the vertical one at the crest.

In the super-critical open-channel flow (Fig.8-(b)), redistribution from vertical to streamwise is observed as well as the wind-driven flow, however spanwise pressure-strain term was almost constant in the vicinity of the free-surface.

In the view points of the free-surface turbulence modeming, the effect of the surface deformation on the vertical turbulent intensity can be considered as giving the sources term at the free-surface corresponded to the value of the vertical turbulent intensity in the super-critical open-channel flow. In the wind-driven flow, turbulent intensity distributions and theirs redistributions in the vicinity air-liquid interfaces are strongly influenced by the wind-wave shapes. Therefore, the spatiotemporal dynamical calculation of wind-waves might be required in the wind-driven flow.

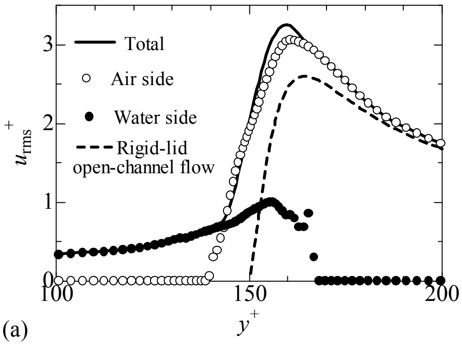

(a)

Streamwise turbulent intensity profiles, near interface
(Wind-driven flow)

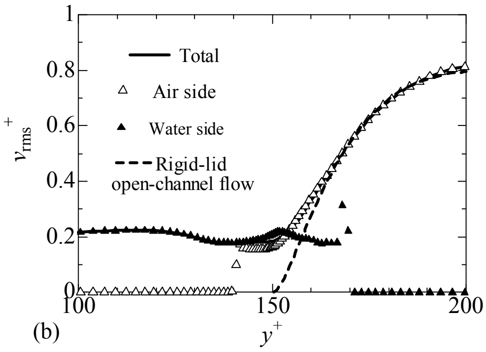

(b)

Vertical turbulent intensity profiles, near interface
(Wind-driven flow)

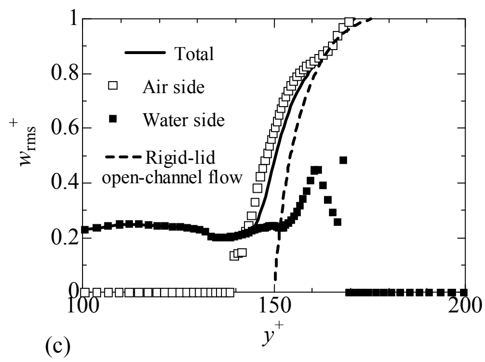

(c)

Spanwise turbulent intensity profiles, near interface
(Wind-driven flow)

Figure 5. Turbulent intensity profies near air-liquid interfaces, wind-driven flow

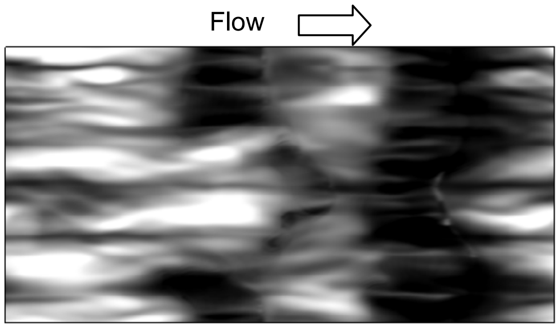

(a) -0.15[m/s](black)<u<0.4[m/s](white), y^{+}=152.6

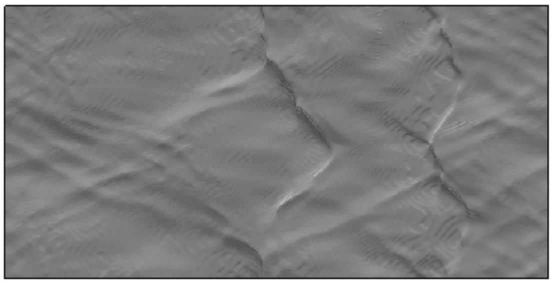

(b) instantaneous interface profile

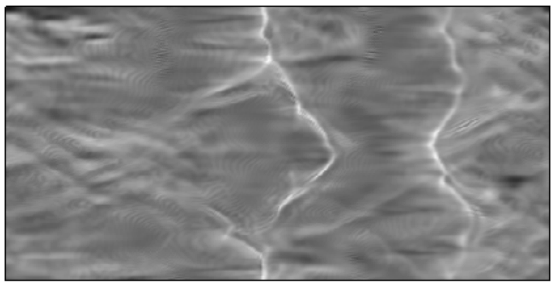

(c) -0.1[m/s](black)<v<0.1[m/s](white)

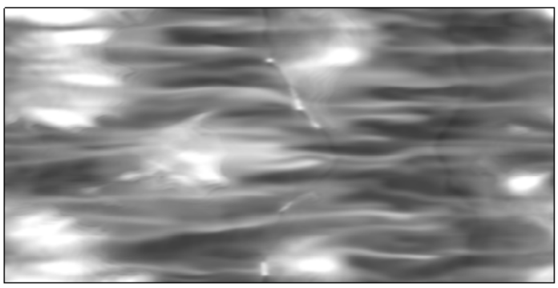

(d) -0.15[m/s](black)<u<0.3[m/s](white), y^{+}=146.4

Figure 6. Flow visualization near air-liquid interface

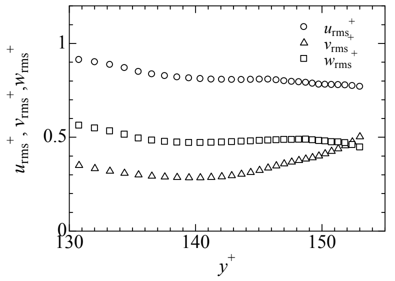

Turbulent intensity profiles, near the free-surface

Figure 7. Water-phase turbulent intensitiy profiles, open-channel flow

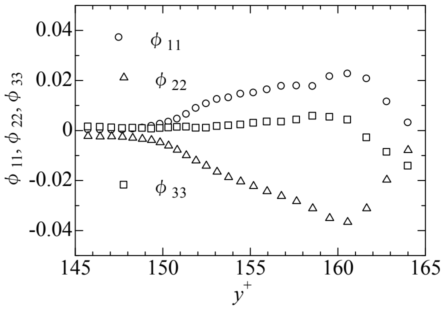

Pressure-strain term profiles, water-side (Wind-driven flow)

(a) wind-drivent flow

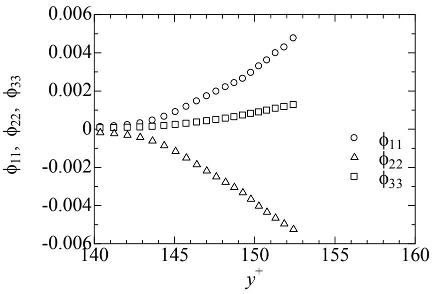

Pressure-strain correlation profiles, near free-surface (Fr=1.8, Water-phase)

(b) open-channel flow

Figure 8.Water-side pressure-strrain term profiles, near air-liquid interface.

CONCLUSION

In the present study, we investigate the effects of a surface deformation on near free-surface turbulent structures, by means of direct numerical simulation (DNS). As the results, we confirm the typical turbulent structures caused by the difference of the origin in surface deformations. In the wind-driven flow, turbulent intensity distributions and theirs redistributions in the vicinity air-liquid interfaces are strongly influenced by the wind-wave shapes. On the other hands, vertical turbulent intensity in the open-channel flow has the peak value on the free-surface and a vertical confinement effect in a low-Fr flow is no longer present in this high-Fr flow.

ACKNOWLEDGEMENT

A part of the present DNS were conducted by using SX-9 at the Cyber Science Center, Tohoku University, and this the study was supported by the Global COE program "Energy Science in the Age of Global Warming"" and a Grant-in-aid for Young Scientists (B), KAKENHI (21760156) MEXT, Japan.

REFERENCES

V. D. Angelis and S. Banerjee,1996, "Direct numerical simulation of near-interface turbulence in coupled gas-liquid flow", Phys. Fluids, vol.8, no.6, pp.1643-1665.

J.U. Brackbill, D.B. Kothe, and C. Zemach, 1992, "A continuum method for modeling surface tension", J. Comput. Phys., 100, pp.335-354.

S. Kawai, 1979, "Generation of initial wavelets by instability of a coupled shear flow and their evolution to wind waves", J. Fluid. Mech., 93, pp.661-703.

S. Komori, H. Ueda, F. Ogino, and T. Mizushina, 1982, "Turbulent structure and transport mechanism at the free surface in an open-channel flow", Int. J. Heat Mass Transfer, 25, pp.513-521.

T. Kunugi, 2001, "MARS for multiphase calculation", Comput. Fluid Dynamics J., 9-1, pp.563-571.

I. Nezu, 2005, "Open-channel flow turbulence and its research prospect in the 21st century," J. Hydraulic Eng., pp .229 -246.

Y. Yamamoto, T. Kunugi and A. Serizawa, 2001, "Turbulence statistics and Scalar Transport in an Open-Channel Flow", J. Turbulence, 2, 010.

Y. Yamamoto, T. Kunugi and S. Satake, 2007, "Surface deformation effects on the free-surface turbulence structure in High-Fr open-channel flow", Turbulent shear flow phenomena 5, 3 ,pp.1223-1228.

Y.Yamamoto and T. Kunugi, 2010, "Direct numerical simulation of a high-Froude-number turbulent open-channel flow", Phyis. Fluids, submitted.